Diurnal variation of outgoing longwave radiation associated with high cloud and UTH changes from Meteosat-5 measurements

Article *in* Meteorology and Atmospheric Physics · October 2009

DOI: 10.1007/s00703-009-0041-8

CITATIONS
15

READS
152

4 authors, including:

Eui-Seok Chung
University of Miami
50 PUBLICATIONS **768** CITATIONS

SEE PROFILE

Johannes Schmetz
None
153 PUBLICATIONS **5,105** CITATIONS

SEE PROFILE

Meteorol Atmos Phys (2009) 105:109–119
DOI 10.1007/s00703-009-0041-8

ORIGINAL PAPER

Diurnal variation of outgoing longwave radiation associated with high cloud and UTH changes from Meteosat-5 measurements

Eui-Seok Chung · Byung-Ju Sohn · Johannes Schmetz

Received: 7 April 2008 / Accepted: 18 August 2009 / Published online: 26 August 2009

Abstract Diurnal variations of outgoing longwave radiation (OLR) are examined in conjunction with diurnal variations of high cloud and upper tropospheric humidity (UTH) over the Indian Ocean and surrounding land areas using Meteosat-5 measurements. Most land areas exhibit a significant diurnal variation of OLR with the largest amplitude over the Arabian Peninsula, whereas the diurnal variation of OLR is much weaker over the Indian Ocean. While diurnal maxima of OLR are found in the early afternoon over many regions of the analysis domain following the diurnal cycle of solar heating, convectively active regions of both land and ocean where high cloud and UTH exhibit distinct diurnal variations show OLR maxima before local noon. These results indicate that high cloud development in the afternoon induces a shift in local time of OLR maxima over convective regions. In agreement with earlier studies it is shown that UTH diurnal variations are less important in regard to their impact on the OLR variations.

1 Introduction

The outgoing longwave radiation (OLR) reflects facets of atmospheric circulation in response to incoming solar radiation. In response to the distinct characteristics of the solar heating cycle, the OLR is expected to show a significant diurnal variation. Considering the fact that OLR has been used to evaluate physics and parameterizations depicted in climate models (e.g., Lin et al. 2000), better understanding of the OLR diurnal variation may facilitate successful modeling of the climate system.

Diurnal variation of OLR has been investigated using polar orbiting satellite measurements (e.g., Raschke and Bandeen 1970). However, those measurements are not sufficient to fully resolve the diurnal variation, since polar orbiting satellites generally provide measurements at two local times on a given day and for a given region (Negri et al. 2002). Although an improved temporal sampling has been achieved by the Earth Radiation Budget Satellite (Barkstrom 1984), longer time periods were required to analyze the diurnal variation, and it is likely that averaging missed some of the time-varying features.

By contrast, superior temporal samplings from geostationary satellites have facilitated the analysis of diurnal variations. Narrowband radiances from Meteosat and GOES satellites have been used to analyze the diurnal variation over the African continent, the Americas, the Atlantic Ocean, and the Pacific Ocean (e.g., Minnis and Harrison 1984; Duvel and Kandel 1985; Schmetz and Liu 1988; Ellingson and Ba 2003; Slingo et al. 2004). Although a broadband radiation budget sensor has been in operation on Meteosat Second Generation in geostationary orbit recently (Harries et al. 2005), narrowband radiance measurements are still indispensable for the study of diurnal variations over various regions, in particular over the Indian Ocean where our understanding of diurnal variation is poorer, in comparison to other regions such as the Pacific Ocean and the Atlantic Ocean (Gambheer and Bhat 2001).

We see the Indian Ocean as an important area from the perspective of meteorology because atmospheric phenomena, such as the Madden–Julian oscillation (MJO) and the

E.-S. Chung (✉) · B.-J. Sohn
School of Earth and Environmental Sciences,
Seoul National University, Sillim-dong,
Gwanak-gu, Seoul 151-747, Korea
e-mail: chunges@eosat.snu.ac.kr

J. Schmetz
EUMETSAT, Darmstadt 64295, Germany

South Asian monsoon, originate there. Despite such an importance, the lack of adequate satellite measurements over the Indian Ocean has hindered us from investigating high-frequency phenomena. In 1998, a European meteorological satellite (Metesoat-5) moved to the Indian Ocean (centered at 63°E) and offered an opportunity of studying variability in the weather and climate over the Indian Ocean (e.g., Roca et al. 2002; Sohn and Schmetz 2004).

It is well known that the distribution and variation of OLR are largely influenced by cloud and water vapor in the upper troposphere (Held and Soden 2000; Sohn and Schmetz 2004; Sohn et al. 2006). However, our understanding of physical processes controlling the diurnal variations of cloud and water vapor in the upper troposphere is still far from being complete. Furthermore, understanding of these physical processes is essential for the better understanding of physics in the climate models, which will then lead to improved climate models. Thus it is of great interest to examine the diurnal variations of high cloud and UTH, and to quantitatively assess their role in the diurnal variation of OLR over the meteorologically important Indian Ocean area. In this study, we intend to examine the diurnal variation of OLR in conjunction with the diurnal variations of high cloud and UTH over the Indian Ocean and surrounding land areas (30°N–30°S, 30°E–110°E) using narrowband radiances of Meteosat-5 for July 1998 and January 1999.

2 Data and analysis methodology

2.1 Data

Radiances from the infrared window (IR, 10.5–12.5 μm) and water vapor (WV, 5.7–7.1 μm) channels of Meteosat-5 were used to estimate OLR, high cloud, and UTH over the Indian Ocean and surrounding land areas. OLR was determined from radiances of IR and WV channels and satellite viewing angle (θ) as in Roca et al. (2002), i.e.:

$$F_{\mathrm{LW}} = a_0 + a_1 L_{\mathrm{IR}} + a_2 L_{\mathrm{IR}}^3 + a_3 L_{\mathrm{IR}}/\cos\theta + a_4 L_{\mathrm{WV}} + a_5 L_{\mathrm{WV}}^2 \quad (1)$$

where F_{LW} is OLR flux (W m^{-2}) and L_{IR} and L_{WV} are the radiances (W m^{-2} sr^{-1}) of the Meteosat-5 IR and WV channels, respectively. The coefficients (a_i, $i = 1,\ldots, 5$) are determined from the collocated longwave fluxes from ScaRaB and Meteosat IR and WV radiances. It was shown that the regression coefficients are stable with time and that longwave fluxes estimated from Metesoat-5 radiances are in good agreement with the ScaRaB observed fluxes with a root mean square error of 10 W m^{-2} (Roca et al. 2002). Equation 1 and associated coefficients were applied to Meteosat-5 measurements for July 1998 and January 1999 in order to convert narrowband radiances into broadband fluxes. OLR data were then produced in a 2.5° × 2.5°-grid format over the analysis domain.

In order to assess the OLR estimated from Eq. 1, we compared monthly mean OLR derived from Meteosat-5 through Eq. 1 with monthly mean OLR observed from the Clouds and the Earth's Radiant Energy System (CERES; Wielicki et al. 1996) onboard Tropical Rainfall Measuring Mission (TRMM) satellite for July 1998. As shown in Fig. 1, comparison indicates that mean bias and RMSE are approximately 2.7 and 4.9 W m^{-2}, respectively. These statistical results do support the validation of using Eq. 1 for estimating OLR from Meteosat-5 radiance observations.

Radiances of IR and WV channels were converted into brightness temperatures (TBs) for the estimation of high cloud and UTH. A value of 260 K for the IR channel TB (TB_{IR}) is used as a threshold for the high cloud fraction as in previous studies (e.g., Tian et al. 2004; Chung et al. 2007). Considering that this temperature threshold approximately corresponds to 440 hPa over the tropics, and that high cloud is defined as cloud whose top pressure less than 440 hPa in the International Satellite Cloud Climatology Project (ISCCP) cloud classification scheme (refer to ISCCP website, http://isccp.giss.nasa.gov/cloudtypes.html), the use of 260 K as a threshold is reasonable for identifying high clouds. For the estimation of UTH, which is defined as a layer mean relative humidity between 500 and 200 hPa over clear sky conditions, the logarithmic relationship proposed by Soden and Bretherton (1996) was applied to the WV channel brightness temperatures (TB_{WV}), i.e.:

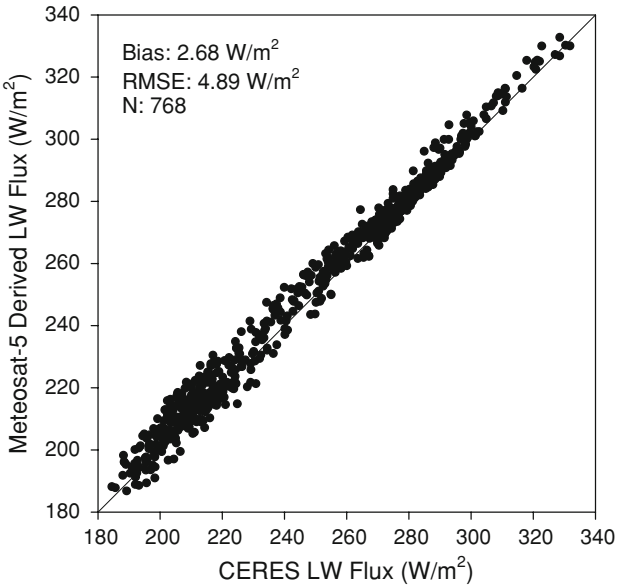

Fig. 1 Comparison of monthly mean OLR derived from Meteosat-5 radiances with monthly mean OLR observed from CERES onboard TRMM for July 1998

$$\mathrm{UTH} = \cos\theta/p_0 \exp(a + b\mathrm{TB_{WV}}) \quad (2)$$

where p_0 represents a reference pressure. The coefficients a and b were determined using a linear regression method with a simulated $\mathrm{TB_{WV}}$. Temperature and humidity profiles in the TIROS Operational Vertical Sounder (TOVS) Initial Guess Retrieval (TIGR) database were inserted into a radiative transfer model (RTTOV-7; Saunders 2002) to simulate the WV channel brightness temperatures. It should be pointed out that UTH estimation is possible only if both high and mid level clouds are absent, because the weighting function of the water vapor channel is near zero below a level of approximately 700 hPa (Brogniez et al. 2006).

2.2 Methodology for diurnal variation analysis

A harmonic analysis is used to study the diurnal variations of OLR, high cloud, and UTH and their relationships. It is assumed that those variables at each local time for a given day and for a given region consist of both a diurnal cycle part and a weather noise part (Duvel and Kandel 1985). While the diurnal cycle repeats periodically as a function of time, weather noise does not repeat on a daily cycle. As a result, it is necessary to smooth out the weather noise part using a large sample size (Duvel and Kandel 1985; Smith and Rutan 2003). In doing so, daily composites are first prepared by averaging those fields at each time step for a 1-month period at each grid point. Then, the amplitude and phase of the first diurnal harmonic are estimated by decomposing the obtained daily composite using Fourier analysis. For example, for a time series of variable y, the amplitude A and phase δ of the diurnal harmonic are defined as follows:

$$y(t) = \bar{y} + A\cos\left[\frac{2\pi}{24}(t-\delta)\right] + \text{residual} \quad (3)$$

where the first term on the right hand side denotes the daily average. The phase of the first diurnal harmonic is given in local time (LT), from which the time showing a local maximum is found.

In addition to harmonic analysis, an empirical orthogonal function (EOF) analysis is used to examine significant spatial and temporal features controlling the diurnal variation of OLR. Since the most dominant varying modes can be extracted with explained variances, EOF analysis is helpful to understand the physical processes associated with the diurnal variation of OLR. The EOFs and associated principal components are computed using the method of Smith and Rutan (2003) and Comer et al. (2007). Because the main part of the analysis domain is over the Indian Ocean, EOF analysis is performed for the whole domain without separating the domain into land and ocean.

3 Diurnal variation of OLR

Figure 2 shows monthly mean OLR for July 1998 and January 1999. Also shown are diurnal amplitudes and phases of OLR. The geographical distributions of OLR (upper panels) clearly show convective regions such as the Indian subcontinent, the Bay of Bengal, Indochina, Ethiopian highlands, and the southern Indian Ocean around 10°S in July 1998, and the area extending from the Maritime continent to southern Africa and Madagascar in January 1999; see the area showing the monthly mean OLR smaller than 240 W m^{-2}. By contrast, longwave fluxes larger than 270 W m^{-2} are observed over the subtropical subsidence regions.

An averaged time series of OLR is decomposed using harmonic analysis at each grid point. The results obtained are displayed using harmonic dials in which the length of an arrow indicates the amplitude of the first diurnal harmonic; see lower panels of Fig. 2. The phase showing a maximum can be determined from the orientation of the arrow with respect to a 24-h clock. For example, upward, right, downward, and left pointing arrows denote the maximum at 00:00 LT (midnight), 06:00 LT (dawn), 12:00 LT (noon), and 18:00 LT (sunset), respectively.

Distributions of amplitude show a clear land–sea contrast. Diurnal amplitudes are generally much larger over land in comparison to those found over the ocean. In particular, desert regions such as the Arabian Peninsula exhibit a large diurnal amplitude up to 35 W m^{-2} in July 1998. Due to the decreased insolation, smaller amplitudes ($\sim$20 W m^{-2}) are found over the same area in January 1999. By contrast, diurnal amplitudes over most of the Indian Ocean are smaller than 5 W m^{-2}, reflecting the generally small diurnal amplitude of sea surface temperature (Webster et al. 1996; Chen and Houze 1997).

OLR reaches a maximum in the early afternoon over deserts. Due to the small heat capacity of desert, the surface quickly heats up during the day. The early afternoon maximum is explained, in part, by the fact that cloud cover and water vapor amounts are insufficient to attenuate the radiation emitted from the surface and the atmospheric boundary layer. The seasonal change of the diurnal phase appears to be small over desert regions. Similar early afternoon maxima are found over southern Africa and Madagascar in July 1998, and the Indian subcontinent and Indochina in January 1999. Monthly mean OLR is relatively larger over those regions.

By contrast, relatively earlier peaks are observed over land where monthly mean OLR is much smaller than 240 W m^{-2}. The Indian subcontinent, Indochina, and Ethiopian highlands in July 1998, and southern Africa and Madagascar in January 1999, exhibit OLR maxima earlier than local noon. Similar diurnal variation characteristics are

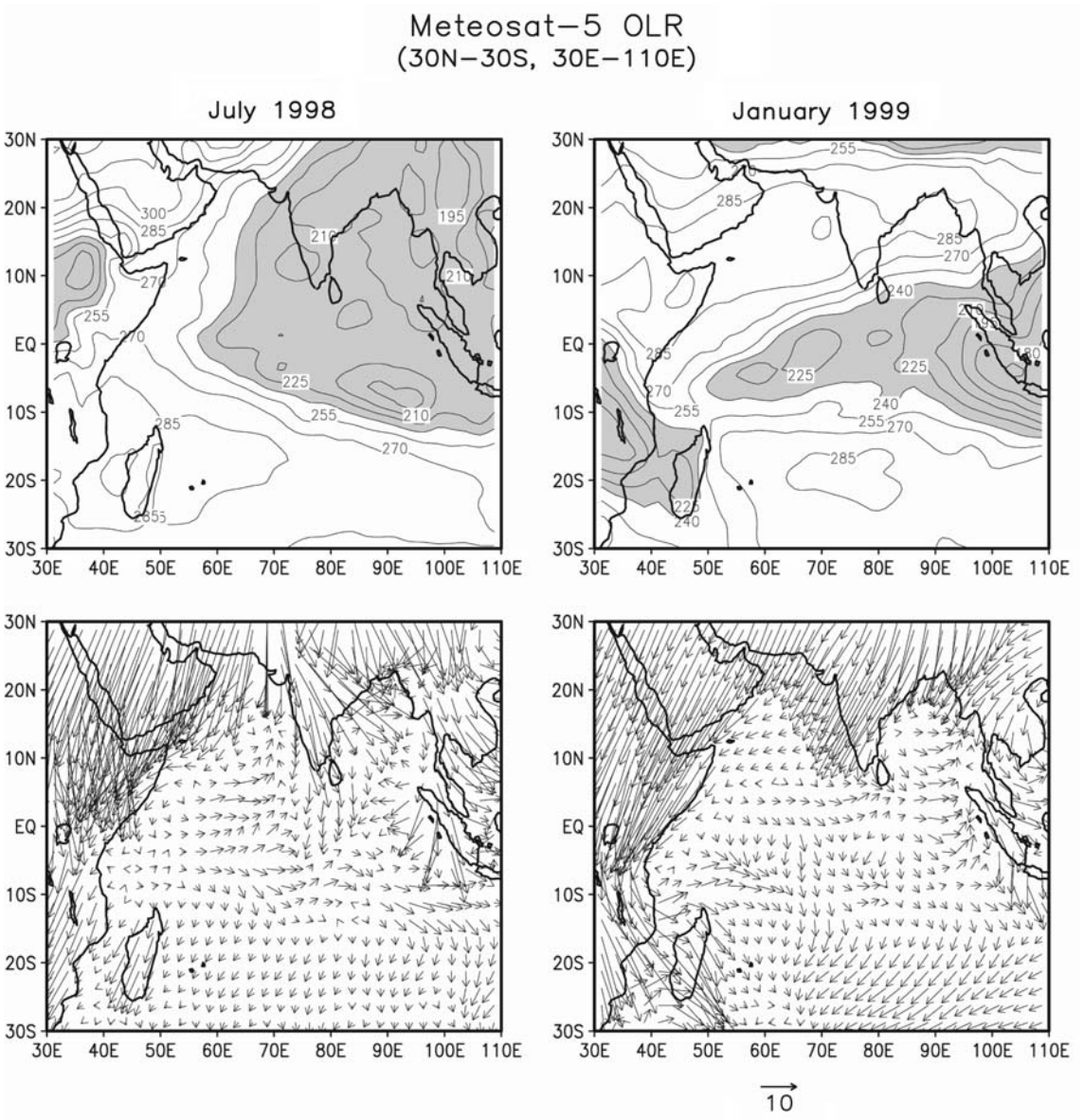

Fig. 2 Geographical distributions of monthly mean OLR (*upper panels*) estimated from Meteosat-5 IR and WV radiances for July 1998 and January 1999. OLR values smaller than 240 W m^{-2} are *shaded* to represent convective regions. *Lower panels* present the diurnal amplitude and phase of OLR. The length and the orientation with respect to a 24-h clock of the *arrow* denote the diurnal amplitude (unit: W m^{-2}) and phase, respectively

observed over Sumatra island for both months. Since high cloud associated with deep convection tends to reach a maximum in the late afternoon to early evening over continental convective regions (e.g., Kondragunta and Gruber 1994; Yang and Slingo 2001; Tian et al. 2004; Chung et al. 2007), the high cloud development in the afternoon appears to be related to earlier OLR maxima over these regions.

Although the diurnal amplitude is much smaller compared to that over land, regional variation of the diurnal phase over the Indian Ocean appears to be significant. More longwave fluxes are emitted into space in the morning over the open oceans between 10°N and 10°S where convection is prevalent, as suggested by the monthly mean OLR field. Chen and Houze (1997) noted that convective cloud systems with a large spatial scale tend to form in the afternoon due to higher sea surface temperatures. Since these systems develop during the night and decay after sunrise, OLR is expected to show a maximum in the morning. The morning peak of OLR is also consistent with findings that oceanic convective regions tend to have minimum high cloud coverage in the morning (Tian et al. 2004; Chung et al. 2007).

Marine stratocumulus (prevailing over the subtropical Indian Ocean) regions exhibit an OLR maximum mostly in

the early afternoon. It is consistent with the results of Schmetz and Liu (1988) which show that the diurnal variation of OLR over marine stratocumulus regions is induced by the diurnal course of solar absorption within the cloud. They argued that the gradual increase of solar absorption in the early part of the day within the clouds leads to the dissipation of clouds during the day, and thereby the minimum stratocumulus amount (and thus maximum OLR) occurs in the afternoon. In line with Schmetz and Liu (1988), Allan et al. (2007) reported approximately identical local time of minima in low-level cloud fraction and maxima in OLR from the observations of Geostationary Earth Radiation Budget (GERB) and the Spinning Enhanced Visible and Infrared Imager (SEVIRI) onboard Meteosat-8 satellite. They also noted the inconsistency between observations and models, pointing at a weakness in the current parameterization of boundary layer clouds in models. Meanwhile, analysis of low-level clouds from the ISCCP D1 dataset (Rossow and Schiffer 1999) shows the smallest cloud coverage at 15:00–16:00 LT over the subtropical Indian Ocean for both months (not shown), which is consistent with Schmetz and Liu (1988) and Allan et al. (2007). A similar diurnal cycle was presented in Kondragunta and Gruber (1994).

The diurnal variation of OLR is relatively complex over the Bay of Bengal in July 1998. Gradual variation of the diurnal phase is shown from coastal regions toward the center of the Bay of Bengal. Similarly the Gulf of Guinea exhibits a series of diurnal phase changes from the coast to the open oceans (Chung et al. 2007). Such complexity seems to be associated with the influence of adjacent lands and the propagation of cloud systems to the ocean as suggested in Yang and Slingo (2001) and Zuidema (2003). By contrast, the diurnal phase is more homogeneous over the Bay of Bengal in January 1999, since convective activities are rare over the surrounding land areas. Considering that OLR diurnal variation is regional, it is noted that the limited sampling of non-geostationary satellites does not well observe the OLR variation and thereby results in biased mean values over longer time scales (Ellingson and Ba 2003). Meanwhile, the new CERES products combined with geostationary imagery (e.g., monthly diurnal mean data) may be used to overcome this limitation (refer to http://eosweb.larc.nasa.gov/GUIDE/dataset_documents/cer_isccp-d2like-geo.html).

Meteosat-5 derived OLR is decomposed into a set of EOFs. The geographical distributions of two leading EOF modes for July 1998 and January 1999 are displayed together with the time series of the corresponding principal component. The first EOF modes, which account for about 86% of the diurnal variation of OLR, exhibit a dominant land–sea contrast (Fig. 3). The most significant signals are found over land such as the Arabian Peninsula and Northeast Africa with large positive values. These regions

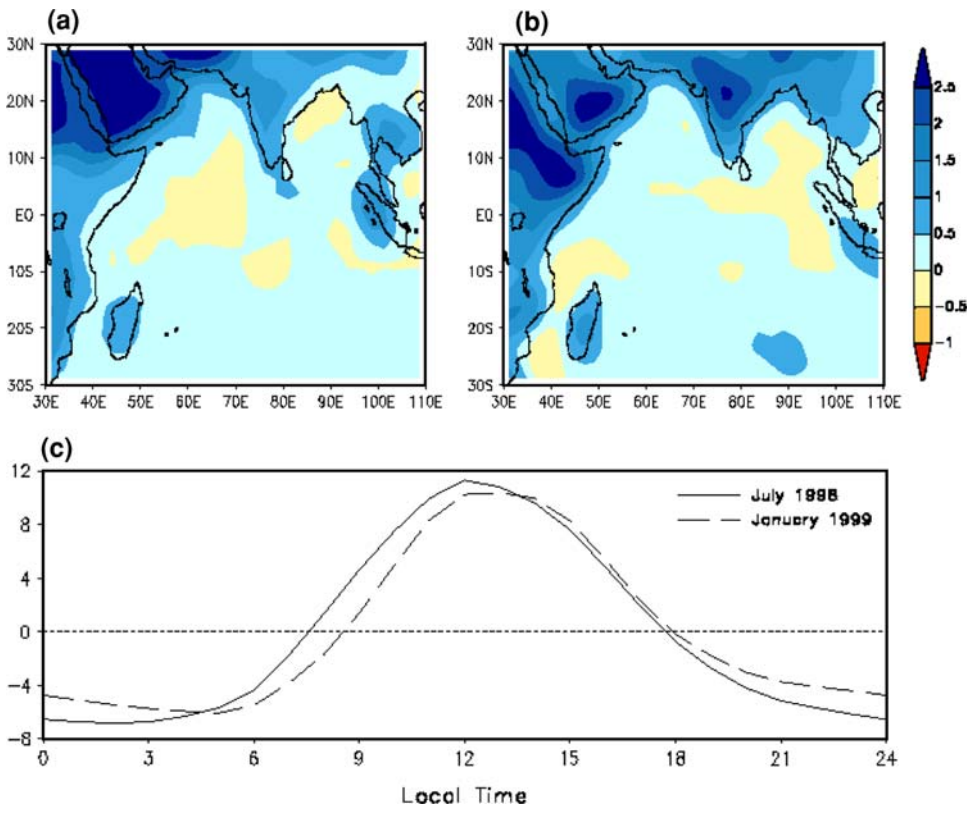

Fig. 3 Spatial patterns of the first EOF mode for OLR: **a** July 1998 (85.4%) and **b** January 1999 (86%). **c** Time series of corresponding principal component for July 1998 (*solid line*) and January 1999 (*dashed line*) [unit: W m^{-2}]

correspond to areas showing the largest diurnal amplitude as noted in Fig. 2. On the other hand, magnitudes are small over the Indian Ocean. The contrast between land and ocean is largely attributable to the different diurnal range of surface temperatures. The associated principal component represents a half sine curve; see lower panel of Fig. 3. OLR rapidly increases after sunrise and reaches a maximum near local noon. By contrast, OLR decreases slowly at night as a consequence of the slow surface radiative cooling. As a result, the first principal component reflects the surface response to the diurnal cycle of solar heating. Considering that most of the analysis domain exhibits positive values in the spatial vector field, the first principal component leads to the OLR maxima around local noon. Thus, the decomposed diurnal phase from harmonic analysis can be explained by the surface heating and cooling due to the diurnal cycle of insolation, especially over dry regions of the Arabian Peninsula and Northeast Africa. However, a lesser degree of diurnal variation is expected over the ocean, in response to the solar heating.

Figure 4 illustrates the geographical distributions of the second EOF mode for July 1998 and January 1999. Also shown is the corresponding principal component for both months. The second EOF mode explains about 12% of the total variance. Thus, the diurnal variations of OLR are almost completely resolved by the first two independent modes. While the first mode represents a clear land–sea contrast, the second mode shows a relatively complex pattern. Positive signs are generally found over convective regions, with larger magnitudes over land. By contrast, non-convective regions tend to show negative signs. Comparison with Fig. 2 indicates that regions with positive signs have an OLR maximum before local noon. Principal components for the second mode show a maximum around 07:00–09:00 LT and a minimum around 18:00 LT.

By combining the first principal component with the spatial vector field of the first mode, it is noted that the OLR maxima occur around local noon. Therefore, the diurnal phases showing the shifted local time (Fig. 2) appear to be due to the processes related to the second EOF mode. In other words, the second EOF mode plays the role of refining the shape of OLR diurnal variations dominated by the first mode (Smith and Rutan 2003; Comer et al. 2007). The combination of the principal component with the spatial vector field for the second mode results in positive signs in the afternoon over deserts and land regions of the winter hemisphere. Positive signs in the afternoon are also found over the subtropical Indian Ocean with a maximum at 18:00 LT, where marine stratocumulus tends to have a minimum extent in the afternoon due to solar absorption within the cloud (e.g., Schmetz and Liu 1988).

By contrast, the second mode exhibits positive signs in the morning over regions showing lower monthly mean OLR. In particular, larger magnitudes are noted over the

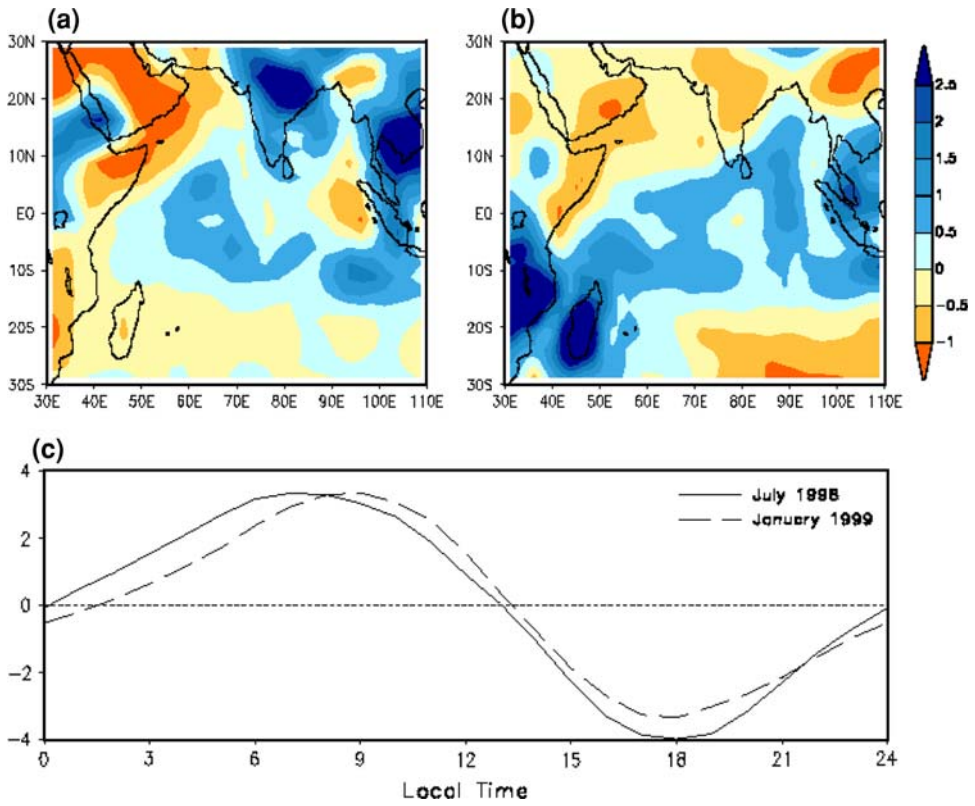

Fig. 4 Spatial patterns of the second EOF mode for OLR: **a** July 1998 (12.6%) and **b** January 1999 (12.4%). **c** Time series of corresponding principal component for July 1998 (*solid line*) and January 1999 (*dashed line*) [unit: W m^{-2}]

Indian subcontinent and Indochina in July 1998, and southern Africa and Madagascar in January 1999. Given the fact that these regions exhibit the OLR maximum before local noon, it is likely that the second mode is associated with the processes responsible for the morning peak of OLR.

4 Influences of high cloud and UTH on the diurnal variation of OLR

It is well known that cloud and water vapor in the upper troposphere are the dominant factors determining OLR over convective regions. Diurnal variation studies have shown that convective regions have distinct diurnal variations of high cloud and UTH (e.g., Udelhofen and Hartmann 1995; Chen and Houze 1997; Tian et al. 2004; Chung et al. 2007). Thus, this section intends to examine diurnal variations of high cloud and UTH in conjunction with the second EOF mode for OLR.

Monthly mean high cloud amount and UTH estimated from Meteosat-5 measurements are presented with shading in Fig. 5. In July 1998, higher cloud amounts are observed over the Indian subcontinent, Indochina, and Ethiopian highlands, and over the tropical Indian Ocean, while broad local maximum UTH areas are found over the tropical Indian Ocean and the Bay of Bengal. In January 1999, the maximum area of high cloud amount and UTH extends from the western Pacific to southern Africa. Such geographical distributions are consistent with the monthly mean OLR pattern. Figure 5 also displays diurnal amplitudes and phases of high cloud and UTH using harmonic dials. High cloud (upper panels) shows large diurnal amplitudes over convective regions where monthly mean cloudiness is high. The maximum cloudiness over continental convective regions, Indonesia, and Madagascar occurs in the late afternoon to midnight (18:00–24:00 LT). Distinct diurnal variations are observed over oceanic convective regions of the Indian Ocean, although their amplitude is smaller. Optically thicker parts of high cloud

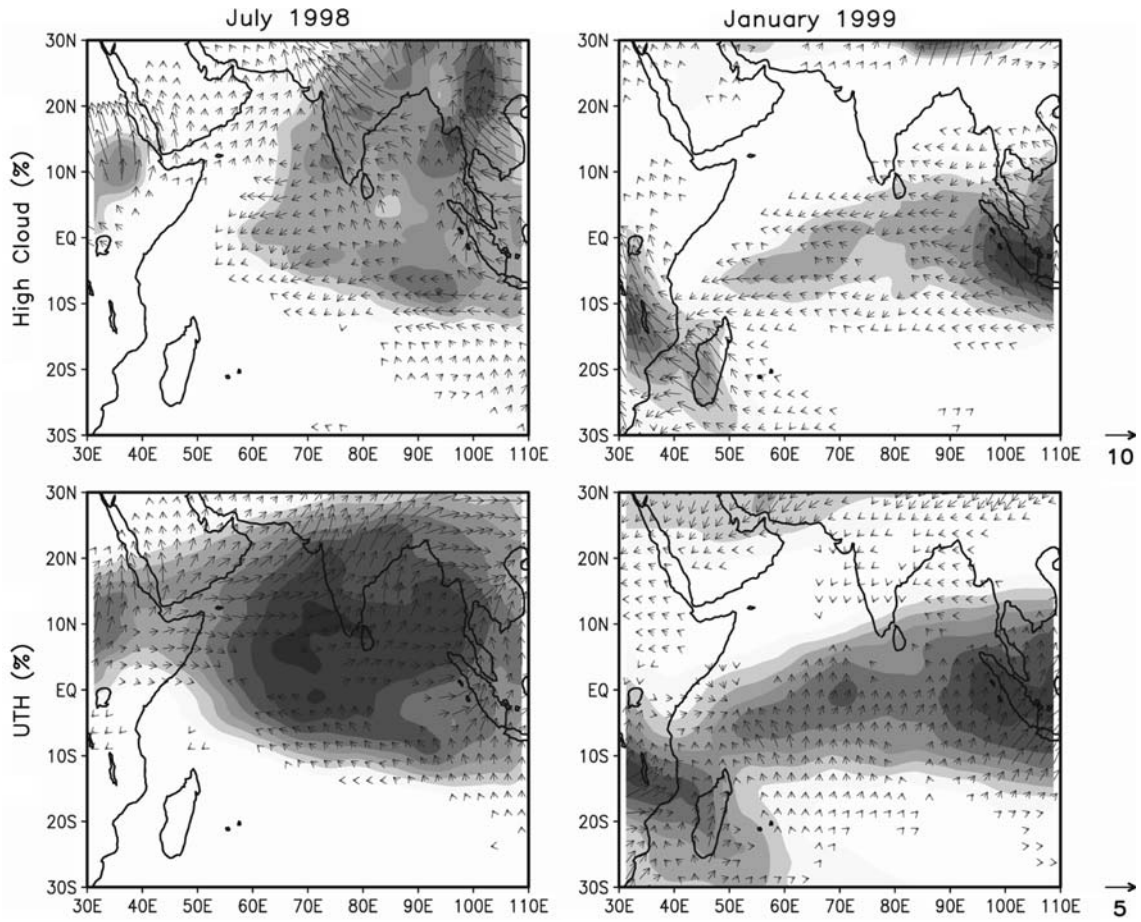

Fig. 5 Diurnal amplitudes and phases of high cloud (*upper panels*) and UTH (*lower panels*) for July 1998 and January 1999. The *length of the arrow* depicts the diurnal amplitude (10% for high cloud and 5% for UTH). *Background shadings* illustrate monthly mean values with higher values denoted by *darker shadings*

tend to peak at ~18:00 LT over the open oceans, suggesting afternoon development of high cloud. Slightly later peaks are noted over coastal regions such as the Bay of Bengal, the Arabian Sea, and the west coast of the Malaysian peninsula and Sumatra. The seasonal difference in the diurnal phase is not significant over both continental and oceanic convective regions. General characteristics of diurnal variations of high cloud are consistent with previous results over other tropical regions (Duvel 1989; Tian et al. 2004; Chung et al. 2007).

A distinct diurnal variation of UTH is observed over convective regions, with a larger amplitude over land (lower panels of Fig. 5). UTH tends to peak between midnight and dawn over the Indian subcontinent, Indochina, and Ethiopian highlands in July 1998, and over southern Africa and Madagascar in January 1999, and over Indonesia for both months. Thus, UTH shows a lagged peak compared to high cloud amount. The diurnal variations of UTH over those regions suggest that less longwave flux is emitted during the night as a result of increased UTH due to decaying high and mid level clouds. In January 1999, higher latitude regions (20°N–30°N) show an afternoon peak. However, the UTH diurnal variation over these high latitude regions does not appear to be robust because of the cold surface temperature and the frequent passage of synoptic weather events.

A noticeable UTH diurnal variation is found over the Indian Ocean. A regional variation of the diurnal phase is significant in July 1998. The UTH maxima occur between late afternoon and midnight over the southern Indian Ocean. By contrast, UTH values over the Arabian Sea and coastal regions exhibit maxima in the early morning, probably due to land influences and moisture advection. In January 1998, the diurnal phase is more homogeneous with UTH maxima between late evening and midnight.

Histograms are constructed to examine the diurnal evolution of high cloud in different layers of the upper troposphere. It was assumed that clouds with lower brightness temperature are located in the upper layer. Numbers of observed IR channel brightness temperatures are counted in 5-K intervals for each time step of a day. Then the diurnal anomalies of the percentage histogram are constructed for areas over land and ocean separately, by subtracting the daily mean percentage histogram. Figure 6 presents the diurnal anomalies of the percentage histogram over land and ocean for July 1998. The histogram over land shows a coherent vertical structure with maximum high-level cloudiness occurring in the late afternoon to early evening (16:00–21:00 LT) for clouds whose top temperature is lesser than 250 K. These clouds are less frequent in the morning (09:00–12:00 LT), enabling the surface and lower atmosphere to emit more longwave flux into space. By contrast, high clouds whose top temperature is greater than 250 K show a lagged peak of occurrence, with maximum occurrence at night (00:00–06:00 LT). Histograms for January 1999 are generally similar to those for July 1998 (not shown).

A clear vertical phase lag is shown in the histogram over ocean. While the coldest portions of high cloud ($TB_{IR} <$ 210 K) peak around 09:00 LT, warmer portions exhibit diurnal minima at the same time. High clouds whose top temperature is around 230 K are more frequent in the late afternoon (15:00–18:00 LT). This maximum time is similar to the diurnal phase shown in Fig. 5, suggesting that the

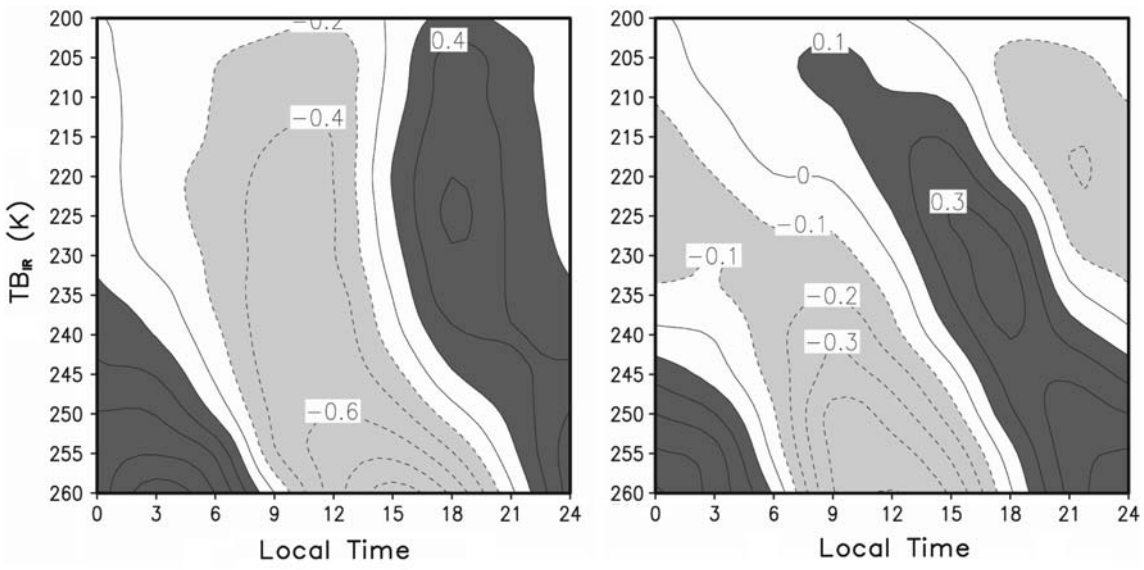

Fig. 6 *Histograms* of the diurnal variation in percentage of grids for which TB_{IR} occurred within each 5-K interval for July 1998. *Contours* denote departures from the daily mean for each bin. *Left and right panels* represent land and ocean, respectively

diurnal phase of high cloud is largely determined by the diurnal variation of these clouds. Warmer clouds ($TB_{IR} > 245$ K) are prevalent throughout the night, and tend to dissipate in the morning. The contrast of vertical phase relations between land and ocean seems to be associated with the disparate convection mechanisms for the open oceans (Gray and Jacobson 1977; Randall et al. 1991; Yang and Smith 2006).

Diurnal anomalies of OLR are compared with those of high cloud and UTH over the regions where the monthly mean OLR is smaller than 240 W m^{-2}. Non-convective regions are excluded since the diurnal variations of high cloud and UTH are not significant over those regions. Furthermore, the surface response to the diurnal cycle of insolation is a dominant factor determining the diurnal variation over those dry regions, as revealed in the first EOF mode. Figure 7 compares the diurnal anomalies for January 1999. Due to different characteristics of diurnal variations, diurnal anomalies are constructed for areas over land and ocean separately. Averaged diurnal anomalies of high cloud are almost 180° out of phase with those of OLR with larger amplitude over land. Since more high cloud reduces infrared emission to space, it is expected that anomalies of high cloud are opposite to OLR anomalies (e.g., Schmetz and Liu 1988; Nowicki and Merchant 2004). High cloud attains maximum cloudiness in the late afternoon to early evening (18:00–21:00 LT) over convective regions of land. Over oceanic convective regions, the high cloud maximum is found in the afternoon (15:00–18:00 LT). Both land and ocean exhibit minimum cloudiness in the morning (land, 09:00–12:00 LT; ocean, 07:00–10:00 LT), indicating high cloud development in the afternoon in association with convective activities. It is noted that approximately similar phase interaction of diurnal variations was documented by Nowicki and Merchant (2004). As a result, less longwave flux can be emitted into space from the surface and lower atmosphere in the afternoon compared to non-convective regions.

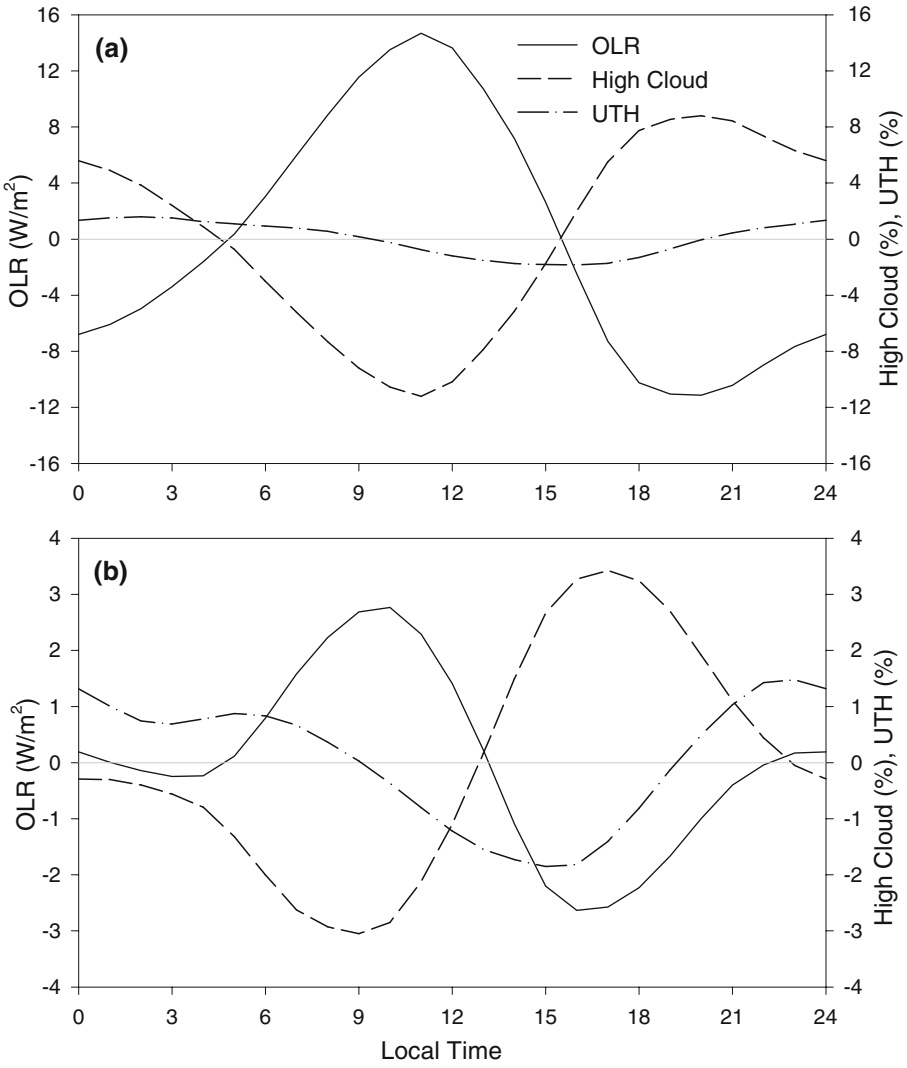

Fig. 7 Diurnal anomalies in OLR (W m^{-2}), high cloud (%), and UTH (%) for spatial averages over convective regions in January 1999: **a** land and **b** ocean. Grid points with monthly mean OLR smaller than 240 W m^{-2} are considered as convective regions

Thus, the local time of OLR maximum is shifted against the diurnal cycle of solar heating.

UTH also shows a noticeable diurnal variation over convective regions. The local time of UTH maximum tends to lag the high cloud maximum by approximately 6 h. UTH peaks around 03:00 LT and has a minimum in the afternoon over land. An earlier peak is noted over oceanic convective regions. Therefore, it is expected that less longwave flux is emitted into space during the night. The relative importance of UTH changes on the OLR has been discussed before. For example, Schmetz et al. (1990) showed in their Fig. 1 that the OLR changes non-linearly by about 20 W m^{-2} when the UTH is changed from 10 to 90%, demonstrating the importance of the UTH for the atmospheric greenhouse effect. However, the radiative effect appears to be minor because the diurnal amplitude of UTH is much smaller than that of high cloud, and because the OLR sensitivity to water vapor change is smaller when the upper troposphere is moister (Held and Soden 2000). Therefore, the influence of UTH change on the OLR variation is not substantial in the diurnal time scale.

5 Summary and conclusions

Meteosat-5 IR and WV channel radiances were used to examine the diurnal variation of OLR over the relatively poorly understood Indian Ocean and surrounding land areas for July 1998 and January 1999. Since cloud and water vapor in the upper troposphere influence the distribution and variation of OLR (Held and Soden 2000; Sohn and Schmetz 2004; Sohn et al. 2006), diurnal variations of high cloud and UTH were examined, in comparison to OLR variation.

A significant diurnal variation of OLR is observed over most land regions, with the largest diurnal amplitude over the Arabian Peninsula. The largest OLR occurs in the early afternoon over most of the analysis domain, mainly due to the response of surface temperature to the diurnal cycle of solar heating. On the other hand, convective regions show an OLR maximum before local noon.

Distinct diurnal variations of high cloud are observed over regions where OLR exhibits maxima before local noon. Minimum cloudiness is found in the morning over both land and oceanic convective regions, suggesting that more longwave flux can be emitted into space from the surface and lower atmosphere in the morning. Convective regions also show distinct UTH diurnal variations with later peaks compared to high cloud. However, the influence of diurnal variations of UTH on the OLR appears to be less important due to their small diurnal amplitude. This study shows again that the diurnal variation of high cloud plays an important role in regulating the diurnal variation of OLR over convective regions.

The fact that this study is based on one summer and one winter month of a strong La Niña year (1998–1999) may have an influence on absolute values of the range of diurnal cycles and the OLR. However, it seems that general features shown in this study are qualitatively robust. For example, Chung et al. (2007) compared the local time of maxima and minima of deep convection, high cloud, cirrus anvil cloud, and upper tropospheric humidity noted in Udelhofen and Hartmann (1995), Soden (2000), and Tian et al. (2004). Although analysis domain and time period were different, their Table 2 indicates that spatiotemporal difference in the diurnal variation is not significant. In spite of the fact that high clouds are not subdivided into optically thicker parts and thinner parts in this study, the phase lag of high clouds and UTH compared to the peak of deep convection is qualitatively consistent with a recent study of Zelinka and Hartmann (2009). Meanwhile, we analyzed the 9-year ISCCP D1 high cloud dataset for July (1998–2006) and January (1999–2007) in order to investigate difference from a kind of climatology, and found that the amplitude and phase of diurnal variation of high cloud are generally consistent with Fig. 5. As a result, it is certain that the results in this study represent the general features associated with the diurnal mode. However, it is desirable to examine how diurnal variations vary with major atmospheric circulation changes associated with El Niño or SST changes in the tropical Indo-Pacific warm pool. Continuous measurements by Meteosat satellites over the Indian Ocean will help to address these questions.

It appears difficult to clearly point out the causes of the diurnal variations of the OLR in all facets, because daily variability of OLR is the integrated result of changes in temperature, cloud, and humidity at the surface and in the atmosphere. Therefore, there is a need to examine the OLR diurnal variation from a different more detailed perspective, for instance, by examining the contribution of different scene types to the regional diurnal variations of OLR (e.g., Schmetz and Liu 1988).

Acknowledgments Authors would like to thank four anonymous reviewers for their constructive and valuable comments which led to an improved version of the manuscript. This work was supported by the SRC program of the Korea Science and Engineering Foundation, and by the NSL program through the Korea Science and Engineering Foundation funded by the Ministry of Education, Science and Technology (S10801000184-08A0100-18410).

References

Allan RP, Slingo A, Milton SF, Brooks ME (2007) Evaluation of the Met Office global forecast model using Geostationary Earth Radiation Budget (GERB) data. Q J R Meteorol Soc 133:1993–2010

Barkstrom BR (1984) The earth radiation budget experiment (ERBE). Bull Am Meteorol Soc 65:1170–1185

Brogniez H, Roca R, Picon L (2006) A clear-sky radiance archive from Meteosat "water vapor" observations. J Geophys Res 111:D21109

Chen SS, Houze RA (1997) Diurnal variation and life-cycle of deep convective systems over the tropical Pacific warm pool. Q J R Meteorol Soc 123:357–388

Chung ES, Sohn BJ, Schmetz J, Koenig M (2007) Diurnal variation of upper tropospheric humidity and its relations to convective activities over tropical Africa. Atmos Chem Phys 7:2489–2502

Comer RE, Slingo A, Allan RP (2007) Observations of the diurnal cycle of outgoing longwave radiation from the geostationary earth radiation budget instrument. Geophys Res Lett 34:L02823

Duvel JP (1989) Convection over tropical Africa and the Atlantic Ocean during northern summer. Part I: interannual and diurnal variations. Mon Weather Rev 117:2782–2799

Duvel JP, Kandel RS (1985) Regional-scale diurnal variations of outgoing infrared radiation observed by Meteosat. J Clim Appl Meteorol 24:335–349

Ellingson RG, Ba MB (2003) A study of diurnal variation of OLR from the GOES Sounder. J Atmos Ocean Technol 20:90–98

Gambheer AV, Bhat GS (2001) Diurnal variation of deep cloud systems over the Indian region using INSAT-1B pixel data. Meteorol Atmos Phys 78:215–225

Gray WM, Jacobson RW (1977) Diurnal variation of deep cumulus convection. Mon Weather Rev 105:1171–1188

Harries JE et al (2005) The Geostationary Earth Radiation Budget Project. Bull Am Meteorol Soc 86:945–960

Held IM, Soden BJ (2000) Water vapor feedback and global warming. Annu Rev Energy Environ 25:441–475

Kondragunta CR, Gruber A (1994) Diurnal variation of the ISCCP cloudiness. Geophys Res Lett 21:2015–2018

Lin X, Randall DA, Fowler LD (2000) Diurnal variability of the hydrologic cycle and radiative fluxes: comparisons between observations and a GCM. J Clim 13:4159–4179

Minnis P, Harrison EF (1984) Diurnal variability of regional cloud and clear-sky radiative parameters derived from GOES data. Part III: November 1978 radiative parameters. J Clim Appl Meteorol 23:1032–1051

Negri AJ, Bell TL, Xu L (2002) Sampling of the diurnal cycle of precipitation using TRMM. J Atmos Ocean Technol 19:1333–1344

Nowicki SMJ, Merchant CJ (2004) Observations of diurnal and spatial variability of radiative forcing by equatorial deep convective clouds. J Geophys Res 109:D11202

Randall DA, Harshvardhan, Dazlich DA (1991) Diurnal variability of the hydrologic cycle in a general circulation model. J Atmos Sci 48:40–62

Raschke E, Bandeen WR (1970) The radiation balance of the planet Earth from radiation measurements of the satellite Nimbus II. J Appl Meteorol 9:215–238

Roca R, Viollier M, Picon L, Desbois M (2002) A multisatellite analysis of deep convection and its moist environment over the Indian Ocean during the winter monsoon. J Geophys Res 107(D19):8012. doi:10.1029/2000JD000040

Rossow WB, Schiffer RA (1999) Advances in understanding clouds from ISCCP. Bull Am Meteorol Soc 80:2261–2287

Saunders R (2002) RTTOV-7 Users guide. EUMETSAT, pp 21

Schmetz J, Liu Q (1988) Outgoing longwave radiation and its diurnal variation at regional scales derived from Meteosat. J Geophys Res 93:11192–11204

Schmetz J, Mhita M, van de Berg L (1990) Meteosat observations of longwave cloud-radiative forcing for April 1985. J Clim 3:784–791

Slingo A, Hodges KI, Robinson GJ (2004) Simulation of the diurnal cycle in a climate model and its evaluation using data from Meteosat 7. Q J R Meteorol Soc 130:1449–1467

Smith GL, Rutan DA (2003) The diurnal cycle of outgoing longwave radiation from Earth Radiation Budget Experiment measurements. J Atmos Sci 60:1529–1542

Soden BJ (2000) The diurnal cycle of deep convection, clouds, and water vapor in the tropical upper troposphere. Geophys Res Lett 27:2173–2176

Soden BJ, Bretherton FP (1996) Interpretation of TOVS water vapor radiances in terms of layer-average relative humidities: method and climatology for the upper, middle, and lower troposphere. J Geophys Res 101:9333–9343

Sohn BJ, Schmetz J (2004) Water vapor-induced OLR variations associated with high cloud changes over the tropics: a study from Meteosat-5 observations. J Clim 17:1987–1996

Sohn BJ, Schmetz J, Stuhlmann R, Lee JY (2006) Dry bias in satellite-derived clear-sky water vapor and its contribution to longwave cloud radiative forcing. J Clim 19:5570–5580

Tian B, Soden BJ, Wu X (2004) Diurnal cycle of convection, clouds, and water vapor in the tropical upper troposphere: satellites versus a general circulation model. J Geophys Res 109:D10101

Udelhofen PM, Hartmann DL (1995) Influence of tropical cloud systems on the relative humidity in the upper troposphere. J Geophys Res 100:7423–7440

Webster PJ, Clayson CA, Curry JA (1996) Clouds, radiation, and the diurnal cycle of sea surface temperature in the tropical western Pacific. J Clim 9:1712–1730

Wielicki BA, Barkstrom BR, Harrison EF, Lee RB III, Smith GL, Cooper JE (1996) Clouds and the earth's radiant energy system (CERES): an earth observing system experiment. Bull Am Meteorol Soc 77:853–868

Yang GY, Slingo J (2001) The diurnal cycle in the tropics. Mon Weather Rev 129:784–801

Yang S, Smith EA (2006) Mechanisms for diurnal variability of global tropical rainfall observed from TRMM. J Clim 19:5190–5226

Zelinka MD, Hartmann DL (2009) Response of humidity and clouds to tropical deep convection. J Clim 22:2389–2404

Zuidema P (2003) Convective clouds over the Bay of Bengal. Mon Weather Rev 131:780–798